Computational modeling of material forming processes / Simulation numérique des procédés de mise en forme

On the identification of a high-resolution multi-linear post-necking strain hardening model

Kristof Denys, Sam Coppieters, Dimitri Debruyne *

Department of Materials Engineering, KU Leuven, Campus Ghent, Gebroeders De Smetstraat 1, B-9000 Gent, Belgium

A B S T R A C T

The Finite Element Model Updating (FEMU) technique is an inverse method that enables to arrive at a complete solution to the problem of diffuse necking of a thick tensile specimen. Conventionally, FEMU relies on the identification of a phenomenological strain hardening law that inherently limits the accuracy of the method due to the predefined character of the adopted strain hardening law. A high-resolution multi-linear post-necking strain hardening model enables to describe more generically the actual strain hardening behaviour. A numerical concept study is used to scrutinise the identification of such a model using FEMU. It is shown that, unlike progressive identification strategies, a global identification strategy followed by a smoothing operation based on area conservation yields sufficiently accurate results. To study the experimental feasibility, the latter strategy is used to identify the post-necking strain hardening behaviour of a thick S690QL high-strength steel. To this purpose, a notched tensile specimen was loaded up to fracture, while the elongation was measured using Digital Image Correlation (DIC). It is shown that the global identification strategy suffers from experimental noise associated with DIC and the load signal.

© 2018 Published by Elsevier Masson SAS on behalf of Académie des sciences.

1. Introduction

In recent years, fracture mechanics is gaining more interest from industry. For example, the line pipe industry aims at an accurate estimation of the amount of deformation high-strength steel can undergo before failure occurs [1–3]. Also the automotive industry is interested in studying the ductile fracture behaviour of advanced high-strength metals [4] during forming [5] and joining [6]. Finite Element modelling strategies are used to predict and understand ductile fracture phenomena. It is well known that this requires the knowledge of the strain hardening behaviour beyond the onset of necking.

To obtain the flow curve beyond the onset of necking, the strain hardening behaviour in the pre-necking region obtained using the conventional method can be extrapolated. However, no guidelines are available to correctly extrapolate the pre-necking stress–strain curve. Some attempts consist in extrapolating the found phenomenological model, which approximates best the pre-necking strain hardening behaviour [7]. Extrapolation, however, is disputable because the post-necking yield curves are obtained without any information from the targeted deformation phase. Hence, this procedure can lead to different and potentially very unsafe results [8,9].

---

* Corresponding author.
  E-mail addresses: kristof.denys@kuleuven.be (K. Denys), Dimitri.debruyne@kuleuven.be (D. Debruyne).

To tackle this problem, several authors have used inverse methods such as Finite Element Model Updating (FEMU) to characterise the stress–strain curve beyond the point of maximum uniform elongation [7,10–12]. The FEMU approach identifies a phenomenological strain hardening law which limits the procedure to fit a prescribed analytical function to the actual strain hardening behaviour of the material. Consequently, FEMU merely yields a best fit resulting in unavoidable errors due to the material's actual strain hardening behaviour. A more flexible strain hardening law can be obtained by a combination of analytical functions [9,13,14]. Even though these combined functions could potentially result in a better approximation of the strain hardening behaviour, a predefined analytical function is still fitted. Moreover, the user is always confronted with the difficult choice between different functions to obtain the best fit for the material under investigation.

To solve the inflexibility of phenomenological strain hardening laws to accurately describe the full plastic strain range, the possibility of characterising a generic analytical function has been investigated in this paper. Because FEMU will be used, the function should consist out of a minimum number of parameters to limit the computational cost. Therefore, the easiest method is to characterise a piecewise linear function, also referred to as a multi-linear function. Kajberg et al. [11] identified a multi-linear function composed out of four linear functions over a plastic equivalent strain ($\epsilon_{\text{pl}}^{\text{eq}}$) range of 0.8. Because a linear function is fitted over a large strain interval, the accuracy of such an approximation is disputable for a wide range of metals. Furthermore, a constraint was applied to limit the strain hardening behaviour to a monotonously positive decreasing slope, which additionally limits the flexibility. Koc et al. [7] progressively identified a multi-linear function. The latter procedure starts with the identification of one linear function, followed by one-by-one addition of other linear functions. However, only two linear functions are identified over an $\epsilon_{\text{pl}}^{\text{eq}}$ interval of 0.66, whereof the accuracy is again questionable.

In this paper, the inverse identification of a high-resolution multi-linear post-necking strain hardening model is investigated. First, different identification strategies are evaluated using a numerical concept study. Finally, the experimental feasibility of the proposed identification strategy is studied by identifying the post-necking strain hardening behaviour of a 10-mm-thick S690QL High Strength Steel (HSS).

2. Methodology and numerical concept study

2.1. Inverse procedure

FEMU has been widely applied to identify the elastoplastic material properties of sheet metal using phenomenological strain hardening laws [11,15–17]. The basic idea of this procedure is to minimise the discrepancy between experimentally measured and numerically computed surface strains while adapting the material parameters. The surface strains are often measured using Digital Image Correlation (DIC) [18].

In this work, the aim is to extract the strain hardening behaviour from the diffuse neck during a tensile test using FEMU. Comparing the experimentally measured and numerically computed surface strain fields over the entire surface of the specimen would result in redundant information because only the strain fields over the necking region will change during a tensile test in the post-necking area. Moreover, comparing both strain fields at exactly the same location is a difficult problem to cope with [15]. The latter issue can be solved by using a notched tensile test coupon as shown in Fig. 1. The deformation will localise in the vicinity of the red dashed lines shown in Fig. 1. As such, instead of using full-field surface data, the average displacement in the X-direction has been extracted on the red dashed lines. The Y position of the extraction lines has been chosen close to the local necking zone to have more sensitivity to the post-necking parameters, resulting in a more accurate identified strain hardening behaviour. In this work, the extraction lines are at 1 mm above and below the centre of the specimen. The local engineering strain e is calculated as:

$$e = \frac{ext_{\text{u}} - ext_{\text{l}}}{L_0} \tag{1}$$

with ext_{u} and ext_{l} being the averaged displacements at the upper and lower extraction lines, respectively, and L_0 the original length between the two extraction lines (represented as the red dashed lines in Fig. 1). The local engineering strain e is merely defined here to have a local measure that can be used in the cost function. Indeed, the difference between the measured and numerically computed local engineering strain, e^{exp} and e^{num} respectively, is used in the following cost function to minimise:

$$C(\mathbf{p})_e = \sum_{i=1}^{m} \left(e^{\text{exp}} - e^{\text{num}} \right)^2 \tag{2}$$

with m the number of load steps and $\mathbf{p}$ the parameter vector containing the unknown parameters in the strain-hardening model. In case of a multi-linear strain hardening model, the unknown parameters are the slopes of the linear functions. The length of the vector $\mathbf{p}$ depends on the resolution of the model, i.e. the interval in terms of plastic equivalent strain spanned by a single linear function.

Identifying the post-necking strain hardening behaviour requires a displacement-driven FE simulation to exclude plastic instability problems. Consequently, not only the local strain e can be minimised in the FEMU procedure, but also the force
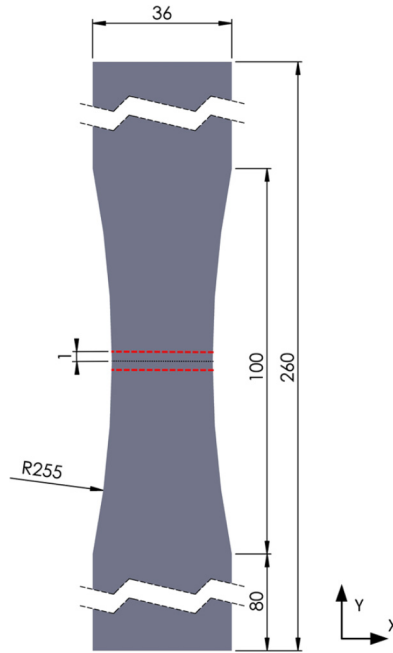
Fig. 1. Notched specimen.

can be included in the cost function to minimise. Decomposing the general cost function in two separate cost functions reads as:

$$C(\mathbf{p}) = C(\mathbf{p})_e + C(\mathbf{p})_F \tag{3}$$

with $C(\mathbf{p})_e$ and $C(\mathbf{p})_F$ the cost functions formed by the local strain component and force, respectively. Because both the force and strain have a different order of magnitude, they are normalised by their experimental value to have the same weight in the general cost function from Eq. (3):

$$C(\mathbf{p})_e = \sum_{i=1}^{m} \left(\frac{e_i^{\text{exp}} - e_i^{\text{num}}}{e_i^{\text{exp}}} \right)^2 \tag{4}$$

$$C(\mathbf{p})_F = \sum_{i=1}^{m} \left(\frac{F_i^{\text{exp}} - F_i^{\text{num}}}{F_i^{\text{exp}}} \right)^2 \tag{5}$$

with F_i^{exp} the experimental force and F_i^{num} the numerical computed force at load step i.

To scrutinise different identification strategies numerically, a tensile test has been simulated in Abaqus/Standard [19] on a 10-mm-thick S690QL notched specimen. The reference strain hardening behaviour used in the FE simulation is a p-model [9] that reads as:

$$\sigma_{\text{eq}} = \begin{cases} K(\epsilon_{\text{pl}}^{\text{eq}} + \epsilon_0)^n & \text{if } \epsilon_{\text{pl}}^{\text{eq}} \leq \epsilon_{\text{max}} \\ K(\epsilon_{\text{max}} + \epsilon_0)^n + Q \left[1 - e^{-p(\epsilon_{\text{pl}}^{\text{eq}} - \epsilon_{\text{max}})} \right] & \text{if } \epsilon_{\text{pl}}^{\text{eq}} > \epsilon_{\text{max}} \end{cases} \tag{6}$$

with σ_{eq} the equivalent von Mises stress, ϵ_0 the initial deformation, n the hardening exponent, ϵ_{max} the maximum uniform strain obtained from a tensile test using a dog bone specimen, p the post-necking strain hardening parameter and Q can be calculated as:

$$Q = \frac{Kn(\epsilon_0 + \epsilon_{\text{max}})^{n-1}}{p} \tag{7}$$

Those parameters have been identified in [12] for the S690QL grade and can be seen as the solid black line in Fig. 2. In the FE simulation, equidistant load steps are chosen with an $\epsilon_{\text{pl}}^{\text{eq}}$ interval of approximately 0.0015. That approximates a DIC measurement where images are taken every second using a cross head speed of 1 mm/min.

In the next paragraphs, the virtually generated experimental data is used to assess the accuracy of three identification strategies in retrieving the reference strain hardening behaviour.
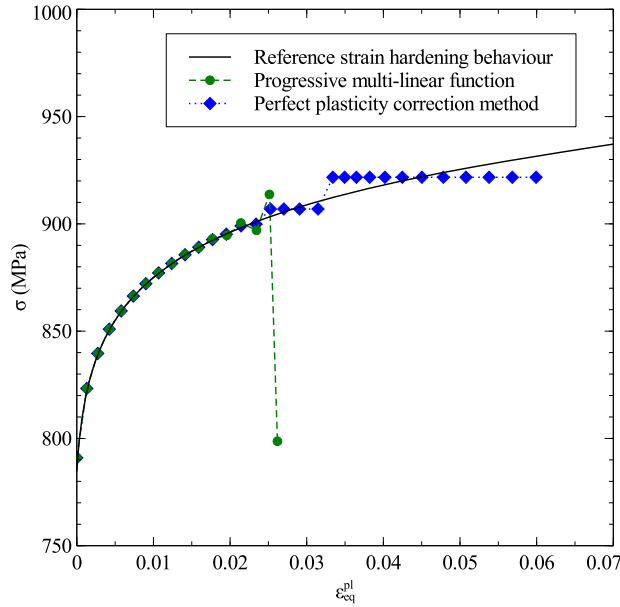
Fig. 2. Identification of a multi-linear function.

2.2. Progressively characterising a multi-linear function

Progressively identifying a multi-linear function has a minimal computation time and has therefore been studied numerically at first. To initiate, a single linear function is identified. Reaching a minimum, a second parameter is added following with one-by-one addition of a linear function each time a minimum has been reached. While identifying a second and an additional linear functions, only the last added linear function has been subjected to identification, which is in contrast with the work of Koc et al. [7], where all parameters remained subjected to identification. The proposed approach could result in a substantial reduction of the computation time because the FE simulation can restart every time from the last identified strain increment. Additionally, less FE iterations are needed to calculate the sensitivity matrix, because only one parameter is subjected to identification.

Adopting this approach results in the green dashed line plotted in Fig. 2. Each load step is visualised as a green circle. It can be seen that the reference strain hardening law is accurately identified up to an ϵ_{pl}^{eq} value of 0.02. Beyond this point, an increasing oscillation of linear functions is observed. Hence, the identification procedure has been stopped at the point where the deviation to the reference hardening law is improbable.

There are three main reasons for the increasing oscillation, all of which related to the number of plastically deforming elements in the FE simulations. First, during the initial linear function identification, all plastically deforming elements in the FE simulation are in the currently identified ϵ_{pl}^{eq} interval. This results in a best fit to the reference strain hardening law. While identifying the following, second linear function, this function needs to compensate for the error made by the first linear function. Because less elements have an ϵ_{pl}^{eq} value inside the second identifying ϵ_{pl}^{eq} interval than during the first one, less elements need to compensate for the error made during the first interval. This phenomenon is plotted as the red dashed line in Fig. 3, where a decreasing number of elements, of which their ϵ_{pl}^{eq} value lies inside the currently identified ϵ_{pl}^{eq} interval, is visualised as a function of ϵ_{pl}^{eq}. As a result, the parameter compensation is enlarged with decreasing numbers of elements inside the identifying ϵ_{pl}^{eq} interval, leading to the observed increasing parameter oscillation.

Second, while identifying the second and following linear functions, more elements are deforming plastically. The new plastically deforming elements deform first according to the first identified linear function. Consequently, an increasing amount of elements are present in the ϵ_{pl}^{eq} intervals former to the identifying interval, which enhances the error and results in another reason for increasing compensation. This phenomenon is shown as the solid black line in Fig. 3, and is the second reason for the enhancing error made during the former intervals, resulting in an increasing oscillation.

Finally, the plastically deforming elements inside each identifying linear function are not always evenly distributed within a plastic equivalent strain interval. Therefore, the weight of the linear function is not averaged over the characterising ϵ_{pl}^{eq} interval. The distribution of some identified linear functions is plotted in Fig. 5 with the normalised ϵ_{pl}^{eq} range $[-0.5; 0.5]$ of the identifying linear function on the x-axis. It can be inferred that for the first linear function the number of elements is more or less evenly distributed. Such distribution would yield a proper identification as schematically shown in Fig. 4A. If the distribution in the second linear function is evenly distributed, also the second linear function will be identified properly, as schematically shown in Fig. 4B. Unlike the first linear function, the sixth linear function exhibits a decreasing amount
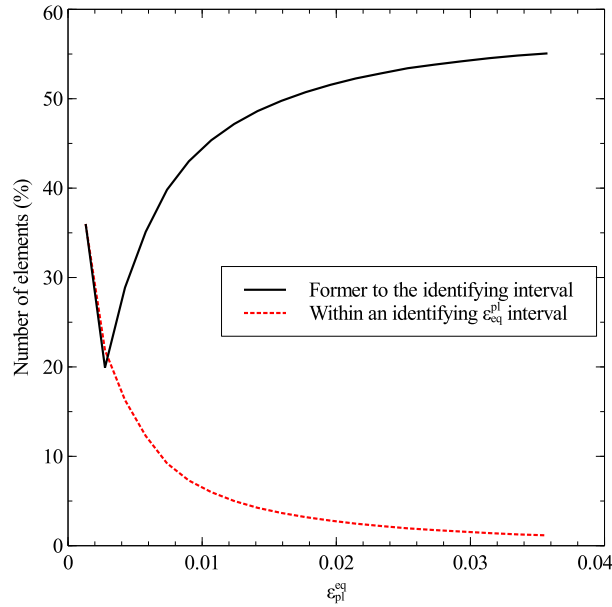
Fig. 3. Amount of FE elements within an ϵ_{pl}^{eq} interval.
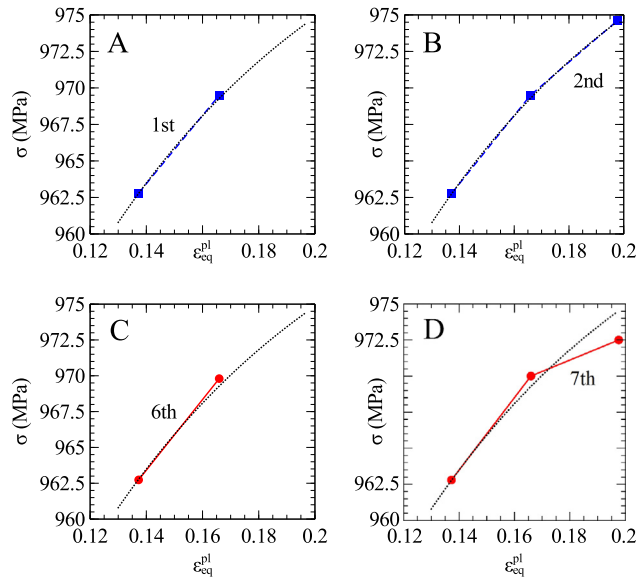

Fig. 4. Characterising difference between an evenly and non-evenly distributed linear function.

of elements at the end of the interval, see Fig. 5. In the latter case, the highest weight of the linear function is located on the onset of the linear function, which would result in the red linear function shown in Fig. 4C. The characterisation of the seventh linear function will have to compensate for the errors made previously, especially if the distribution is again non-evenly distributed. The latter would result in an erroneous identification, as shown in Fig. 4D.

To limit the oscillation, the strain hardening behaviour has been limited to perfect plasticity. This is an acceptable limitation since most materials do not exhibit softening. The result of this limitation can be observed in Fig. 2 as the blue dashed line. At small plastic strains, the reference hardening law is well approximated, while at larger strains, the error increases.

2.3. Progressively characterising a multi-linear function for each FE element separately

In this section, each FE element can have a different strain hardening behaviour. Consequently, a multi-linear function has been progressively identified for each FE element separately. The final strain hardening behaviour can be obtained by
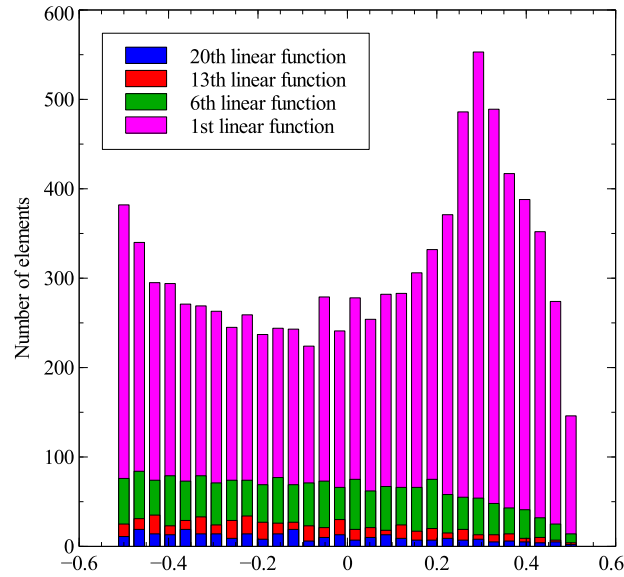
Fig. 5. Distribution of the plastically deforming elements inside a linear function to characterise.
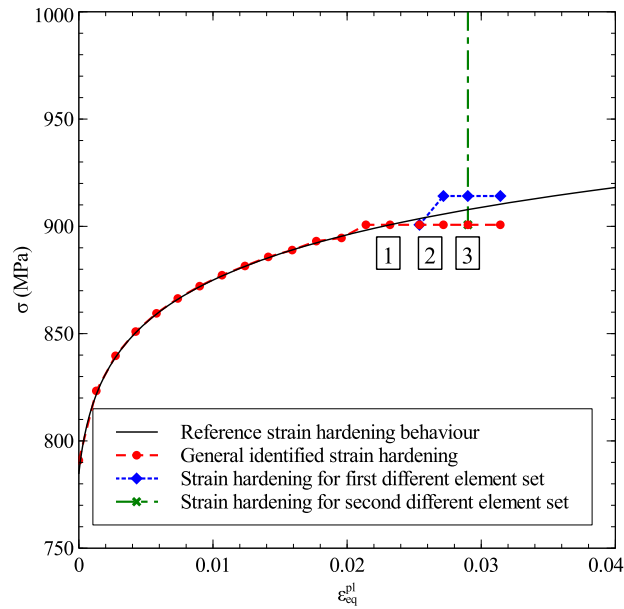

Fig. 6. Identification of a multi-linear function with different element properties.

averaging all the separate linear functions according to the number of elements imposed with a specific strain hardening behaviour. Further, to exclude a negative slope of a linear function, a constraint of perfect plasticity has been employed.

To initiate, an equal multi-linear function is characterised for all the FE elements up to point 1 in Fig. 6. Next, a perfect plastic function is identified (from point 1 up to 2) followed by an increasing strain hardening identification plotted as the dotted blue line. Because only some FE elements deform plastically within this ϵ_{pl}^{eq} interval (after point 2), only these elements are imposed with the increasing function. Subsequently, they retain their perfect plasticity value during the rest of the identification process. The FE elements that did not deform plastically in that ϵ_{pl}^{eq} interval retain their perfect plastic behaviour up to another increasing strain hardening is identified, as can be observed at point 3. However, at this point, an unrealistic strain hardening behaviour is identified, which can be attributed to the number of plastically deforming FE elements, as explained in section 2.2.

It can be concluded that progressively identifying a multi-linear function, or any other function via FEMU, will result in the identification of an oscillating strain hardening behaviour.

2.4. Globally characterising a multi-linear function

In this section, a multi-linear function consisting out of eight linear functions will be identified simultaneously, denoted as a global approach. Kajberg et al. [11] used this approach; however, in this section, no constraints and more linear functions over a smaller $\epsilon_{\mathrm{pl}}^{\mathrm{eq}}$-interval will be used to have a more accurate approximation of the reference strain hardening behaviour. Only the post-necking deformation will be subjected to identification to limit the number of unknown parameters. The pre-necking region can be obtained from the reference strain hardening behaviour in the numerical concept study, while during an actual experiment, the conventional method on a dog bone can be used.

The generally and in previous sections used optimisation algorithm for FEMU, namely Levenberg–Marquardt [7,12,15], is not adequate for identifying eight parameters simultaneously. Therefore, a Nelder–Mead algorithm will be used [20]. This minimisation algorithm is used to find the local minimum of a function with n variables. It is based on the comparison of function values at the $n + 1$ vertices of a generalised simplex, where the vertex can expand and contract till a minimum is found. The main disadvantage is that more iterations are needed to reach a minimum, while it is possible to identify more parameters simultaneously in comparison with the Levenberg–Marquardt algorithm. To minimise the number of iterations, an Adaptive Nelder–Mead Simplex (ANMS) algorithm [21] has been implemented and used in this work.

The identification procedure starts at an $\epsilon_{\mathrm{pl}}^{\mathrm{eq}}$ of 0.05, which is the point of maximum uniform elongation [12]. To have a good initial guess for the multi-linear function, the procedure starts with the characterisation of one linear function over the entire identifying $\epsilon_{\mathrm{pl}}^{\mathrm{eq}}$ interval, visualised as the dotted green line in Fig. 7. Next, the linear function has been divided into eight equidistant linear functions. Then, the procedure minimises simultaneously the eight linear functions, whereof the result is visualised as the red dashed line in Fig. 7. It can be seen that the function does not follow a smooth path, instead an oscillating curve around the reference curve has been characterised.

To reduce the oscillation, a smoothing operation can be applied, which is based on area conservation [22]. The method preserves the integral of the function, while iteratively smoothing the multi-linear function, which consists of m vectors $\mathbf{p}(\epsilon_{\mathrm{pl}}^{\mathrm{eq}}, \sigma)$. The endpoint vectors are not modified by this method, which is an advantage for the starting vector, but a disadvantage for the ending vector due to the large deviation to the former linear functions. Therefore, the ending vector has been ignored during the smoothing procedure. Further, the smoothing operation proposed by Kuprat et al. [22] is only valid for vectors whereof the coordinates have the same order of magnitude. In case of a stress–strain curve, there is a substantial difference in order of magnitude between the stress and strain values. Therefore, they have been normalised by their Root Mean Square (RMS) value before starting the smoothing procedure, as can be found in Eq. (8). After the smoothing operation, the normalised smoothed vectors have been multiplied by their initial RMS values, shown in Eq. (14). Underneath, the modified algorithm is summarised.

1. Calculate the RMS value $\mathbf{p}_{RMS}$
2. Normalise all $\mathbf{p}$:

$$\mathbf{p}_i^n = \frac{\mathbf{p}_i}{\mathbf{p}_{i,RMS}} \tag{8}$$

3. Do $(i = 0, .., m - 4)$ up to convergence:
   (a) Calculate the unit normal $\hat{n}$ whereby $\perp$ is a counterclockwise rotation of 90 degrees:

$$\hat{n} = \frac{(\mathbf{p}_{i+3}^n - \mathbf{p}_i^n)^{\perp}}{\|(\mathbf{p}_{i+3}^n - \mathbf{p}_i^n)^{\perp}\|} \tag{9}$$

   with $\mathbf{p}^{\perp} = (-\sigma, \epsilon_{\mathrm{pl}}^{\mathrm{eq}})$
   (b) Calculate the area of the squad A_i:

$$A_i = \frac{1}{2}\left[(\mathbf{p}_{i+3}^n - \mathbf{p}i^n)^{\perp}(\mathbf{p}_{i+2}^n - \mathbf{p}i^n) + (\mathbf{p}_{i+2}^n - \mathbf{p}i^n)^{\perp}(\mathbf{p}_{i+1}^n - \mathbf{p}i^n)\right] \tag{10}$$

   (c) Calculate the new height h:

$$h = -\frac{3}{2}\frac{A_i}{\|(\mathbf{p}_{i+3}^n - \mathbf{p}i^n)^{\perp}\|} \tag{11}$$

   (d) Calculate the two new positions of $\mathbf{p}_{i+1}^n$ and $\mathbf{p}_{i+2}^n$:

$$\mathbf{p}_{i+1}^n = \frac{2}{3}\mathbf{p}_i^n + \frac{1}{3}\mathbf{p}_{i+3}^n + h\hat{n} \tag{12}$$

$$\mathbf{p}_{i+2}^n = \frac{1}{3}\mathbf{p}_i^n + \frac{2}{3}\mathbf{p}_{i+3}^n + h\hat{n} \tag{13}$$
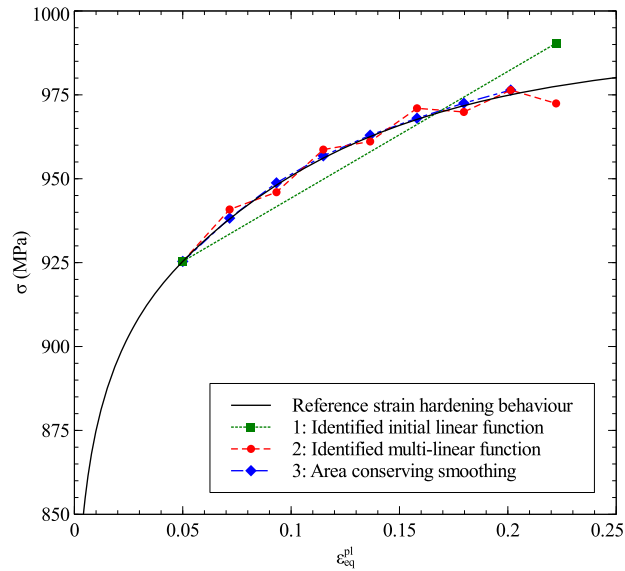
Fig. 7. Global identification of a multi-linear function using a p-model as reference strain hardening model.
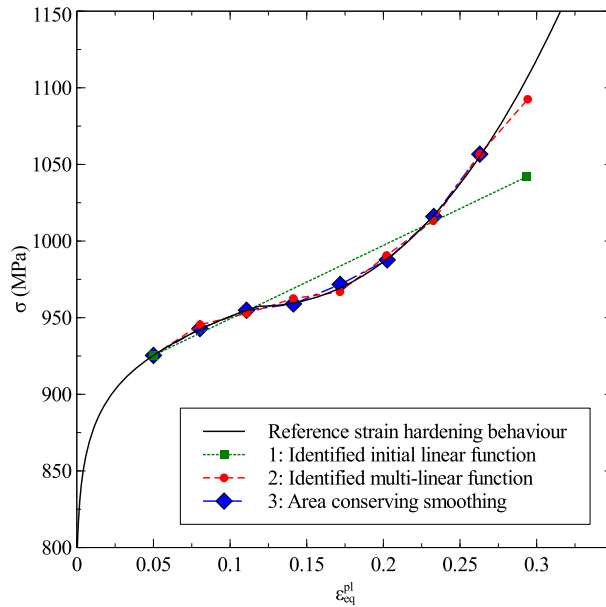

Fig. 8. Global identification of a multi-linear function using a random function as the reference strain hardening model.

4. Recalculate the normalised positions to the actual values:

$$\mathbf{p}_i^{\text{smooth}} = \mathbf{p}_i^n \mathbf{p}_{i,\text{RMS}} \tag{14}$$

The smoothed multi-linear function can be seen in Fig. 7 as the blue dash-dotted curve, where a satisfying agreement can be found with the reference curve.

To examine the level of adaptability of the global approach, a random strain hardening, which is plotted as the black solid line in Fig. 8, has been characterised. First, a single linear function has been identified, visualised as the green dotted line. Next, a multi-linear function has been identified and can be seen as the red dashed line in Fig. 8. Finally, the blue dash-dotted line represents the finally obtained smoothed multi-linear function. A satisfying agreement has been found using the proposed method and two different strain hardening behaviours. It can be concluded that the proposed method could be generic for the strain hardening identification of a large collection of materials.

Table 1
Specification of the DIC parameters in ROI A.

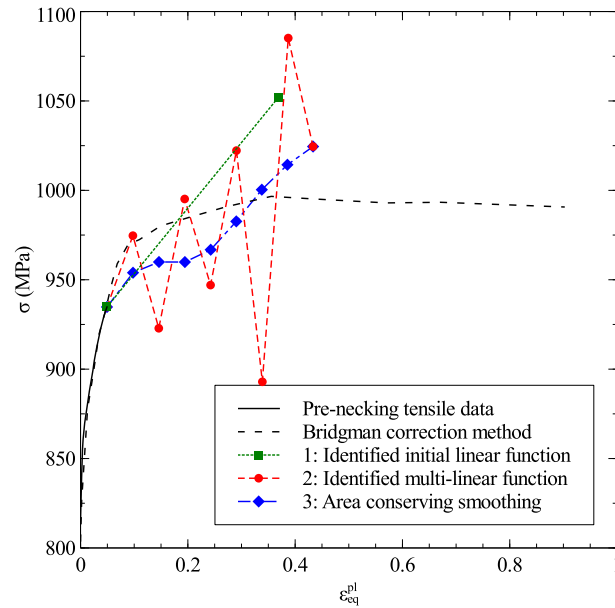| DIC implementation	Specification
Matching criteria	ZNSSD
Interpolation	Bicubic Interpolation
Transformation	Affine
Subset	21 pixels
Step	1 pixel
Displacement resolution	$6.33 \cdot 10^{-4}$ pixels
Strain Smoothing	Bilinear Interpolation
Strain window size	7 Datum points
Strain resolution	$1.14 \cdot 10^{-3}$

Fig. 9. Identification of a multi-linear function on a notched specimen of 10-mm-thick S690QL.

3. Experiments

3.1. Benchmark of the strain hardening behaviour

The global identification approach presented in section 2.4 identifies a multi-linear function starting from the point of maximum uniform elongation. Therefore, the strain hardening behaviour prior to that point needs to be known. Therefore, a tensile test has been performed on a dog bone specimen machined from a 10-mm-thick S690QL grade. A Zwick Z250 tensile equipment has been used with a load capacity of 250 kN equipped with wedge grips. The test was displacement driven with a constant cross head speed of 0.5 mm/min to obtain a quasi-static tensile test. During the tensile test, a stereo DIC setup has been employed to obtain the surface displacement fields. The optimal settings for the DIC parameters can be found in Table 1. From the synchronised DIC measurement and load cell, the strain hardening behaviour can be calculated; it is shown in Fig. 9 as the solid black line.

To have an approximation for the post-necking strain hardening behaviour, a Bridgman experiment has been performed on a round bar specimen [23]. The corrected strain hardening behaviour is shown as the dashed black line in Fig. 9. It should be noted, however, that the Bridgman correction method can include substantial errors in the corrected strain hardening behaviour due to some difficult measurable parameters [12,24].

3.2. Global identification of a high-resolution multi-linear post-necking hardening model

Having measured the strain hardening behaviour prior to necking, the global identification procedure from section 2.4 can be applied on a 10-mm-thick S690QL HSS notched specimen. The tensile test has been performed using the same equipment and conditions as those mentioned in section 3.1.
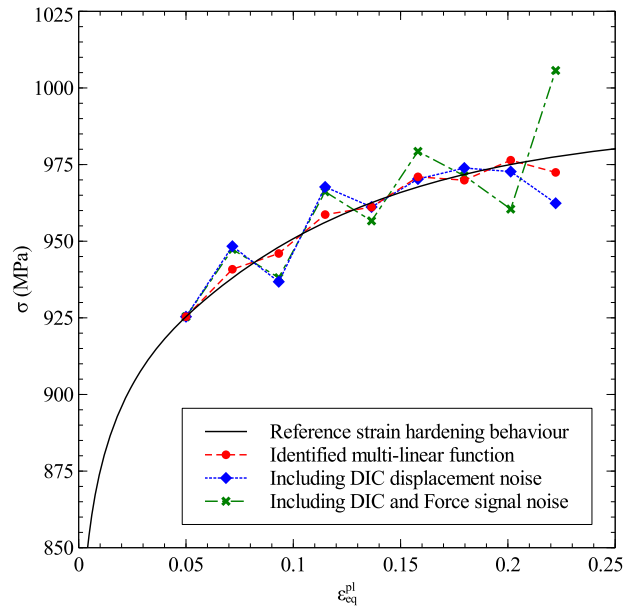
Fig. 10. Result of including noise in the numerical data during the global identification of a multi-linear function on a p-model strain hardening law.

Because DIC [18] is used to obtain the displacement fields, the displacement components near the grips have been extracted along the X and Y directions. Next, they are applied as boundary condition in a displacement-driven FE simulation [12]. This FE simulation is then used in the FEMU procedure to identify the multi-linear function.

First, a linear function has been identified and is shown as the green dotted line in Fig. 9. Next, a multi-linear function has been identified and can be seen as the red dashed curve. Applying the proposed smoothing method on this curve results in the blue dash-dotted curve, which is an unrealistic strain hardening behaviour compared to the strain hardening behaviour obtained with the Bridgman correction method.

It can be inferred from Fig. 9 that the identified linear strain hardening function is a strongly oscillating curve, which has also been found in the numerical concept study. The oscillation magnitude, however, is substantially larger than in the numerical concept study of section 2.4. The latter is scrutinised in the next section.

3.3. Analysis of the oscillating curve

The numerical concept study on the global approach did not include noise associated with the DIC measurement and the analogue force output of the tensile equipment. Nevertheless, both are present during an actual experiment and could potentially lead to the oscillating curves. Therefore, DIC and force signal noise have been added to the numerical concept study. First, DIC noise has been added to the numerical displacement data which has been obtained from the experiment from section 3.2. A Gaussian noise distribution has been measured, with a mean value of $-9.636 \cdot 10^{-4}$ mm and a standard deviation of $5.6 \cdot 10^{-4}$ mm. The global identification result is plotted in Fig. 10 as the blue dotted line. It can be seen that including the DIC noise amplifies the oscillation of the characterised multi-linear function.

Next to the DIC noise, noise on the force output signal is also present during an actual experiment. To obtain this noise distribution, 1000 data points have been measured, while the force level was preserved on the tensile equipment. Three different force levels have been measured, of which all the measurements revealed a normal distribution with a mean value of 112.25 N and a standard deviation of 597.51 N. As an example, the distribution of the force at 20 kN, together with the calculated normal distribution is plotted in Fig. 11.

This noise has been added to the numerical force signal in the numerical concept study. The characterised function including DIC and force signal noise is plotted as the green dash-dotted line in Fig. 10. The same tendency can be found between the oscillation of the numerically characterised green dash-dotted line from Fig. 10 and the experimentally characterised green dashed line from Fig. 9. It can be concluded that noise underlies the experimentally characterised oscillation of the multi-linear function.

4. Conclusion

Different approaches for the identification of a multi-linear post-necking strain hardening model have been scrutinised in a numerical concept study. First, progressively characterising a multi-linear function failed, because compensating the error made in the preceding linear functions was enhanced by the decreasing number of elements in the ϵ_{pl}^{eq} interval under identification. Furthermore, the non-evenly distribution of the plastically deforming FE elements inside some of the ϵ_{pl}^{eq}
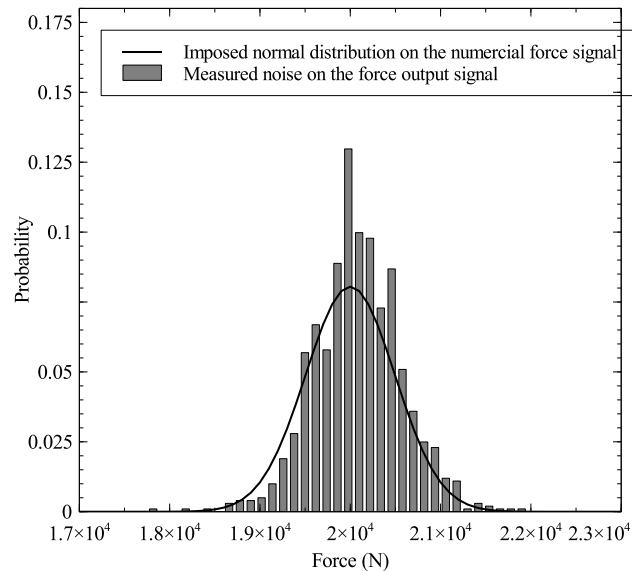
Fig. 11. Measurement of the noise on the force output signal.

intervals also resulted in an increasing oscillation of the multi-linear function. Constraining the multi-linear functions to a minimum of perfect plasticity did not resolve the oscillating problem.

The numerical concept study showed that a global identification approach in which all linear functions are simultaneously identified yields sufficiently accurate results. Application of this approach to an actual experiment, however, resulted in a strongly oscillating strain hardening behaviour. It has been shown that the DIC and force signal noise underlay this problem. We conclude that the global identification of a high-resolution multi-linear post-necking strain hardening model using FEMU will be difficult to apply experimentally, because noise will always be present during an actual experiment.

Acknowledgements

References

[1] R. Ghajar, G. Mirone, A. Keshavarz, Ductile failure of X100 pipeline steel – experiments and fractography, Mater. Des. 43 (2013) 513–525.
[2] C.-K. Oh, Y.-J. Kim, J.-H. Baek, Y.-P. Kim, W. Kim, A phenomenological model of ductile fracture for API X65 steel, Int. J. Mech. Sci. 49 (2007) 1399–1412.
[3] W. Guo, H. Dong, M. Lu, X. Zhao, The coupled effects of thickness and delamination on cracking resistance of X70 pipeline steel, Int. J. Press. Vessels Piping 79 (2002) 403–412.
[4] J. Lian, M. Sharaf, F. Archie, S. Münstermann, A hybrid approach for modelling of plasticity and failure behaviour of advanced high-strength steel sheets, Int. J. Damage Mech. 22 (2012) 188–218.
[5] Y. Korkolis, B. Brownell, S. Coppieters, T. Haobin, Modeling of hole-expansion of aa6022-t4 aluminum sheets with anisotropic non-quadratic yield functions, J. Phys. Conf. Ser. 734 (2016) 032083.
[6] S. Coppieters, H. Zhang, X. Fan, N. Vandermeiren, A. Breda, D. Debruyne, Process-induced bottom defects in clinch forming: simulation and effect on the structural integrity of single shear lap specimens, Mater. Des. 130 (2017) 336–348.
[7] P. Koc, B. Stok, Computer-aided identification of the yield curve of sheet metal after onset of necking, Compos. Mater. Sci. 31 (2004) 155–168.
[8] D. Debruyne, S. Cooreman, D. Lecompte, H. Sol, D. Van Hemelrijck, Identification of the stress–strain behaviour of a tensile specimen after necking, in: Proceedings of the SEM Annual Conference and Exposition, 2006.
[9] S. Coppieters, T. Kuwabara, Identification of post-necking hardening phenomena in ductile sheet metal, Exp. Mech. 54 (2014) 1355–1371.
[10] Y. Ling, Uniaxial true stress–strain after necking, AMP J. Technol. 5 (1996) 37–48.
[11] J. Kajberg, G. Lindkvis, Characterisation of materials subjected to large strains by inverse modelling based on in-plane displacement fields, Int. J. Solids Struct. 41 (2004) 3439–3459.
[12] K. Denys, S. Coppieters, M. Seefeldt, D. Debruyne, Multi-dic setup for the identification of a 3d anisotropic yield surface of thick high strength steel using a double perforated specimen, Mech. Mater. 100 (2016) 96–108.
[13] K. Denys, S. Coppieters, R. Van Hecke, S. Cooreman, D. Debruyne, Identification of a 3d anisotropic yield surface of x70 pipeline steel using a multi-dic setup, in: Proceedings of the 2016 11th International Pipeline Conference, September 26–30, Calgary, Alberta, Canada, 2016.
[14] S. Hertele, W. De Waele, R. Denys, M. Verstraete, Full-range stress–strain behaviour of contemporary pipeline steels, part 1: model description, Int. J. Press. Vessels Piping 92 (2012) 34–40.
[15] S. Cooreman, Identification of the Plastic Material Behaviour Through Full-Field Displacement Measurements and Inverse Methods, Ph.D. Thesis, University of Brussels (VUB), 2008.
[16] D. Lecompte, S. Cooreman, S. Coppieters, J. Vantomme, H. Sol, D. Debruyne, Parameter identification for anisotropic plasticity model using digital image correlation, Eur. J. Control 18 (3) (2009) 393–418.
[17] T. Pottier, F. Toussaint, P. Vacher, Contribution of heterogeneous strain field measurements and boundary conditions modelling in inverse identification of material parameters, Eur. J. Mech. A, Solids 30 (2011) 373–382.

[18] MatchID, MatchID Software, http://www.matchidmbc.com, 2016.

[19] Simulia, Abaqus/standard, version 6.13.

[20] J. Nelder, R. Mead, A simplex method for function minimization, Comput. J. 7 (1965) 308–313.

[21] F. Gao, L. Han, Implementing the Nelder–Mead simplex algorithm with adaptive parameters, Comput. Optim. Appl. 51 (2010) 259–277.

[22] A. Kuprat, A. Khamayseh, D. George, L. Larkey, Volume conserving smoothing for piecewise linear curves, surfaces, and triple lines, J. Comput. Phys. 172 (2001) 99–118.

[23] P. Bridgman, Studies in Large Plas Flow and Fracture, McGraw–Hill, New York, 1952.

[24] G. Mirone, A new model for the elastoplastic characterization and the stress–strain determination on the necking section of a tensile specimen, Int. J. Solids Struct. 41 (2004) 3545–3564.